Fully Automatic 3D Segmentation of Iceball for Image-Guided Cryoablation

Xinyang Liu[1], Kemal Tuncali[1], William M. Wells III[1], *Member, IEEE*, Paul R. Morrison[1], and Gary P. Zientara[1]

Abstract— The efficient extraction of the cryoablation iceball from a time series of 3D images is crucial during cryoablation to assist the interventionalist in determining the coverage of the tumor by the ablated volume. Conventional semi-automatic segmentation tools such as ITK-SNAP and 3D Slicer's Fast Marching Segmentation can attain accurate iceball segmentation in retrospective studies, however, they are not ideal for intraprocedure real time segmentation, as they require time-consuming manual operations, such as the input of fiducials and the extent of the segmented region growth.

In this paper, we present an innovative approach for the segmentation of the iceball during cryoablation, that executes a fully automatic computation. Our approach is based on the graph cuts segmentation framework, and incorporates prior information of iceball shape evolving in time, modeled using experimentally-derived iceball growth parameters. Modeling yields a shape prior mask image at each timepoint of the imaging time series for use in the segmentation. Segmentation results of our method and the ITK-SNAP method are compared for 8 timepoints in 2 cases. The results indicate that our fully automatic approach is accurate, robust and highly efficient compared to manual and semi-automatic approaches.

I. INTRODUCTION

The standard cryoablation procedure consists of a Planning Phase, a Probe Placement Phase and a Therapy Phase. During the Planning Phase, an initial planning scan session, typically x-ray CT or MRI, displaying the anatomy and tumor is acquired prior to probe insertion. These images are used to select and mark a safe skin entry site for the percutaneous probe insertion. Then, depending on the tumor size, from two to five cryoprobes (average three) are sequentially inserted, interdispersed with repeated imaging to confirm proper placement.

The Therapy Phase would typically consist of two 15 min freeze cycles, separated by a 10 min thaw period. During the

freeze cycle, monitoring images are acquired at approx 90-270 sec intervals. In the first freeze cycle, the ablation iceball starts to grow from near the probe tip depending upon probe construction. Fig. 1 illustrates the growing iceball for three types of Galil Medical Inc. (Arden Hills, MN) probes (at our hospital only Galil IceSeed and IceRod probes are used for MRI cryoablations). In this work, we focus on determining the spatial extent of the segmented iceball occurring during the first freeze cycle of kidney tumor ablations.
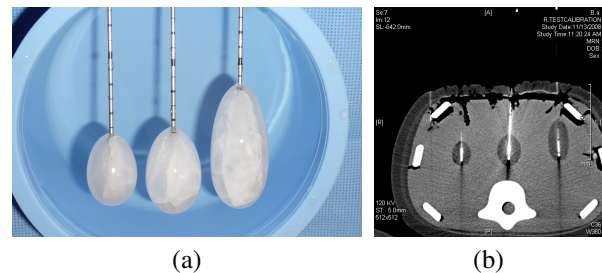

Fig. 1. Three probe types of Galil Medical Inc. (Arden Hills, MN) (from left to right): IceSeed, IceSphere, IceRod. (a) Photo shows iceball formed with probes in room temperature water. (b) CT image of 10 min freeze in a CIRS Inc. (Norfolk, VA) Image Guided Abdominal Biopsy Phantom composed of gel.

Currently, the performance of cryoablations relies entirely on the interventionalist's observations, experience and the interpretation of the image evidence at hand. To forgo the complete reliance of the interventionalist on limited qualitative visual assessment of ablation progress during cryoablation, we first need to create computer software assessing the progress of the therapy by segmenting the ablated volume, in the form of the iceball, from images in a fully automatic, accurate and rapid manner. This segmented iceball can then be compared to the ultimate planned therapy volume composed of tumor and a margin to judge progress at any timepoint in the procedure.

Intraprocedural imaging for kidney tumor ablations at our hospital employs the multi-plane T2-weighted MRI, the breath-hold half-Fourier acquisition single-shot turbo spin echo (HASTE) (3 mm slice thickness) sequence. While radiological advantageous, HASTE images introduce some difficulties for iceball segmentation in that the anatomy surrounding the iceball, especially the probes, have similar intensity values as the iceball, causing any segmentation that relies on intensity information to fail. Semi-automatic segmentation tools such as ITK-SNAP (www.itksnap.org) [1] and 3D Slicer's (www.na-mic.org) Fast Marching Segmentation [2] can attain accurate iceball segmentation in retro-

spective studies, however, their required manual operations are not ideal for real time segmentation intraprocedurally when the interventionalist has higher priority to patient health responsibilities.

In this work, we describe our method, named *GC-prior*, to segment the iceball, formed during cryoablation, in a fully automatic way, at each timepoint during the initial freeze cycle. The approach is based on graph cuts segmentation framework, which has the advantage of fast computation, global optimization and low sensitivity to initialization. Graph cuts was first introduced by Greig et al. [3], and was enhanced when Boykov and Kolmogorov proposed an efficient max-flow/min-cut algorithm [4] and further applied to N-d image segmentation by Boykov and Funka-lea [5]. Our work's key contribution is to incorporate shape information into the segmentation, so that each of the individual iceball's segmentations is initiated with and biased toward the shape modeled using experimentally derived parameters, such that the actual iceball can be separated from the surrounding anatomy having similar intensity values. Unlike Malcolm et al.'s work [6], which equipped the graph cuts framework with shape prior information calculated from a training data set, we directly model the growth of the iceball to predict a reasonable shape prior mask image at each timepoint of the cycle. The reason why an approach based upon use of a training data set may not work in cryoablations is that the type of the probes, the number of probes used and the placement and direction of probe insertion differs significantly from case to case. We compared the segmentation results of GC-prior method with ITK-SNAP method for 8 timepoints in 2 cases, and the results indicate the proposed approach is accurate and robust.

II. GRAPH CUTS AND SHAPE PRIOR

The two-terminal ($s-t$) graph construction in a conventional graph cut scenario is as follows. Each pixel (voxel) in a 2-D (3-D) image is represented by a node in the graph. Besides these 'regular' nodes, there are two special nodes called 'terminals'. One terminal is the source (s), usually standing for foreground, and the other terminal is the sink (t) representing background. Each regular node is connected to the two terminals via two edges, which are referred to as 't-links'. Neighboring regular nodes are connected by edges called 'n-links' according to certain connectivity rules. Each edge is assigned a nonnegative weight, representing the maximum flow capacity through this edge. The graph can be divided into two parts by deleting a set of edges so that each part contains one of the terminals. The cost of a cut is defined to be the sum of the edge weights in the removed set.

Let $\mathscr{P}$ be the set of all non-terminal nodes. The labeling f corresponding to a cut naturally defines a Markov Random Fields (MRF) type of energy

$$E(f) = \lambda \cdot \sum_{p \in \mathscr{P}} R_p(f_p) + \sum_{(p,q) \in \mathscr{N}} B_{p,q}(f_p, f_q) \quad (1)$$

where f_p is the label for node p and $\mathscr{N}$ is the local neighborhood. Function R_p refers to the regional term, which reflects

the penalty of assigning node p to label f_p. Function $B_{p,q}$ is the boundary term that penalizes discontinuities between neighboring nodes. The coefficient $\lambda \geq 0$ specifies a relative importance of the regional term versus the boundary term. Thus, the minimum of energy (1) corresponds naturally with the global optimum of a segmentation.

According to the max-flow/min-cut theory, the minimum cut in a $s-t$ graph equals the maximum flow from s to t. There are many algorithms to find the maximum flow. Boykov and Kolmogorov proposed an efficient augmenting paths algorithm [4] based on searching two trees (rooted at s and t respectively) dynamically. In [4], the regional term is defined to be the negative log-likelihood of a pixel's fit into user-initialized intensity histograms

$$R_p(O) = -\ln P(I_p|O) \quad R_p(B) = -\ln P(I_p|B) \quad (2)$$

where O refers to the foreground and B refers to the background in a binary image. The boundary term is given by

$$\sum_{(p,q) \in \mathscr{N}} B_{p,q} = \exp\left(-\frac{(I_p - I_q)^2}{2\sigma^2}\right) \cdot \frac{1}{\|p-q\|} \quad (3)$$

if $f_p \neq f_q$. σ is a user defined scale parameter and $\|p-q\|$ is the Euclidean distance between two voxels.

Several previous studies have incorporated the shape prior information into the graph cuts energy function, by adding a shape prior function either to the boundary term [7], or to the regional term [6]. In [6], Malcolm et al. generated shape priors using kernel principle component analysis based on a set of training data. Their corresponding regional terms is given as

$$R_p(O) = -(1-\mu)\ln P(I_p|O) - \mu \ln P(O_p) \quad (4)$$
$$R_p(B) = -(1-\mu)\ln P(I_p|B) - \mu \ln P(B_p) \quad (5)$$

where $P(O_p)$ and $P(B_p)$ are the shape priors for the foreground and background, respectively, and $0 \leq \mu \leq 1$ is a parameter to adjust the relative shape influence.

III. PROPOSED GC-PRIOR ALGORITHM

The general idea of our approach is to follow Malcolm et al.'s framework, and to generate the shape priors in a innovative and suitable way for our tasks. Rather than using a training data set, we predict the shape priors based on modeling the iceball's growth utilizing image information from the Baseline scan (the last set of 3D acquisition images at the end of the Probe Placement Phase) and known experimentally-derived parameters for the iceball growth in time.

We first model the growth of the iceball during the first 15 min freeze. Two Galil Medical Inc.'s probes, types-IceSeed and IceRod, are considered here for MRI-guided cryoablations. To derive our iceball growth parameters, we manually measured the size of the iceball for each type of probe at four timepoints-3, 6, 10, 15 min, based on a set of x-ray CT images taken when the probes were inserted into a CIRS abdominal gel phantom (Fig. 1(b)). Since the contour of the iceball for one single probe can be approximated as

a prolate ellipsoid (see Fig. 2(b)), three measurements are recorded: the length of major axis L and minor axis l, and the distance (the shortest) from the intersection of the ellipsoid and the major axis to the tip of the probe, which is denoted as h. The centroid of the ellipsoid can be determined as the point on the probe with its distance to the tip of the probe being $(L/2 - h)$. For each measurement, the four collected values are fitted with a second order polynomial curve to estimate measurements for all timepoints.

The equation of a prolate ellipsoid centered at the origin of a Cartesian coordinate system is

$$\frac{x^2 + y^2}{(l/2)^2} + \frac{z^2}{(L/2)^2} = 1 \qquad (6)$$

which can be rewritten in terms of two distances d_1 and d_2

$$\frac{d_1^2}{(l/2)^2} + \frac{d_2^2 - d_1^2}{(L/2)^2} = 1 \qquad (7)$$

where d_1 is the distance to the major axis and d_2 is the distance to the centroid of the ellipsoid. We use equation (7) to create a prolate ellipsoid mask image for each probe at a given timepoint as shown in Fig. 2(b) and (c), and then combine all individual masks together to form a combined shape mask image (Fig. 2(d)).
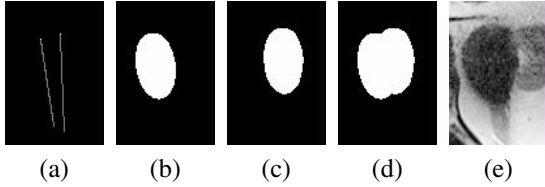

(a)　　　(b)　　　(c)　　　(d)　　　(e)

Fig. 2. An example of predicted shape prior mask image at 15 min. (a) Labeled probes in the Baseline scan. (b) Prolate ellipsoid mask for the left probe. (c) Prolate ellipsoid mask for the right probe. (d) Combined shape prior mask. (e) Corresponding region in the patient's image at 15 min.

In a shape prior mask image, the foreground is labeled as an intensity of 1 and background intensity is set to be 0. Let f be the function giving the label of a point p in the image. The shape prior in (4) is given by a hyperbolic sine-shaped function

$$P(O_p) = \begin{cases} \min(\frac{0.5}{\max(T_0)^2} \cdot T_0^2(p) + 0.5, 1) & \text{if} \quad f(p) = 1 \\ \max(-\frac{0.5}{N^2} \cdot T_1^2(p) + 0.5, 0.001) & \text{if} \quad f(p) = 0 \end{cases}$$
$$(8)$$

where T_0 and T_1 are the Euclidean distance transform to the background and foreground, respectively, in the shape prior mask image, and N is a threshhold such that $P(O_p) = 0.001$ if $T_1(p) \geq N$. $P(O_p)$ in function (8) is between 1 and 0.001, and equals 0.5 for points on the iceball boundary. The value of this function decreases rapidly when the point is far from the boundary and changes slowly near the boundary, in order to let the segmentation be mainly driven by the intensity information in the region around the boundary. When the (background) point is a great distance from the boundary, its shape prior is set to be very small (0.001).

$P(I_p|O)$ in equation (4) is defined to be

$$P(I_p|O) = \exp\left(-\frac{(I_p - I_O)^2}{2\sigma^2}\right) \qquad (9)$$

where σ is the same parameter as in (3) and I_p is the intensity value at voxel p. I_O is the intensity centroid for label O and is learned as the mean intensity value of foreground voxels in the 1 minute shape prior mask image. $P(I_p|B)$ in (5) can be defined in a similar manner. The normalizing constant for the Gaussian distribution has been neglected here for convenience. Now the regional terms (4) and (5) can be expressed as

$$R_p(O) = (1 - \mu) \cdot \frac{(I_p - I_O)^2}{2\sigma^2} - \mu \cdot P(O_p) \qquad (10)$$

$$R_p(B) = (1 - \mu) \cdot \frac{(I_p - I_B)^2}{2\sigma^2} - \mu \cdot P(B_p) \qquad (11)$$

where $P(O_p)$ is given in (8) and $P(B_p) = 1 - P(O_p)$.

The complete algorithm is summarized as follows:

1) Label the probes and identify the tips of the probes in the Baseline scan. (In this study, this is accomplished manually. However, we plan to automate this initial step via use of the 3D Hough transform.)
2) Generate 1 min shape prior mask to learn the intensity centroids.
3) For each timepoint, first create a prolate ellipsoid mask for each probe according to equation (7), and then combine the individual masks together to form a combined shape prior mask image.
4) Calculate the shape prior based on the mask image according to equation (8).
5) Embed the shape prior into the regional terms as in equations (10) and (11), and run the Boykov-Kolmogorov graph cuts algorithm with the boundary term as in (3).

IV. EXPERIMENTS AND DISCUSSION

We performed validation experiments at 8 timepoints in 2 cases-A and B, from real-time MRI-guided and monitored kidney tumor ablations to compare our GC-prior algorithm with the ITK-SNAP semi-automatic segmentation tool. All scans were taken using a 3T wide-bore MRI scanner (Siemens Verio; Erlangen, Germany) with multichannel abdominal coils. Multiplane T2-weighted imaging using breath-hold half Fourier acquisition single shot turbo spin echo (HASTE) sequence was used. Both cases used Galil Medical Inc. IceRod probes and patients had a good breath-hold capability. Motion artifacts between timepoints are neglected, so that inter-scan registration is assumed. Case A consist of three probes and five timepoints in the first freeze, i.e., 3, 6, 9, 12, 15 min. Case B has five probes and three timepoints in the first freeze, at 5, 10, 15 min. The images were first pre-processed with histogram equalization and then resliced and resampled to have isotropic voxels with 1mm resolution.

All the experiments were performed using our GC-prior method with the same parameter values, which were determined experimentally, and thus no manually parameter adjustment was needed. The algorithm was implemented using C++, and execution time for the whole image ($340 \times 290 \times 60$) was about 15 seconds on a modern PC.

An example of the iceball segmentation for case A at 6 min of the first freeze is shown in Fig. 3. For comparison, the manual segmentation result shown in Fig. 3(d) was generated by labeling the iceball manually slice by slice using the ITK-SNAP manual segmentation tool. Fig. 3(e) shows the result of ITK-SNAP semi-automatic segmentation using region competition snakes, requiring manual input and operation. For comparison, we also include in this experiment the segmentation result using 3D Slicer's Fast Marching Segmentation Module, which is shown in Fig. 3(f). This tool is also semi-automatic. Fig. 3(h) shows the result of a naive standard graph cuts segmentation operating without the benefit of the shape prior we introduced here.
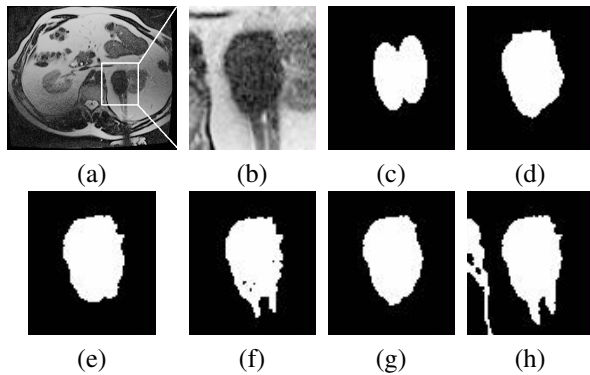

Fig. 3. Segmentation of the iceball for case A at 6 min of the first freeze. (a) Original scan with region shown in zoomed view of this figure. (b) Close-up view of the iceball. (c) Predicted shape prior mask. (d) Result of manual segmentation. (e) Result of ITK-SNAP semi-automatic segmentation using region competition snakes. (f) Result of 3D Slicer's Fast Marching Segmentation Module. (g) Result of GC-prior automatic segmentation method. (h) Result of standard graph cuts segmentation without the shape prior.

The overlap between the (semi)-automatic segmentations and the manual segmentation was computed using the Dice Similarity Coefficient ($D(X,Y) = 2|X \cap Y|/(|X| + |Y|)$), and is shown in Fig. 4. Although our GC-prior method is fully automatic for the segmentation problem at each timepoint, its mean Dice Similarity Coefficient of the 8 timepoints is only slightly lower than the ITK-SNAP semi-automatic segmentation, which therefore indicates its accuracy.

From these experiments, it is notable that both ITK-SNAP semi-automatic segmentation and 3D Slicer's Fast Marching Segmentation require manual intervention to perform each timepoint's segmentation. These semi-automatic methods tend to include the location/shape information through manual input strategies. These approaches can attain high accuracy in retrospective studies, however, they become difficult and time-consuming for real time segmentation, in the case of cryoablations. In contrast, GC-prior method incorporates shape influence into the segmentation automatically at each
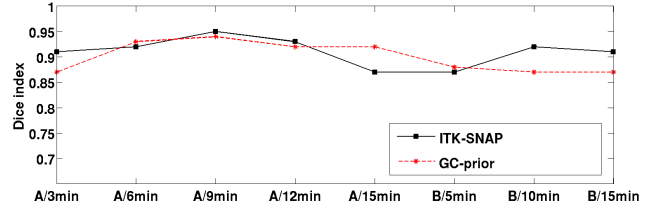

Fig. 4. Dice Similarity Coefficient of ITK-SNAP semi-automatic segmentation and GC-prior automatic segmentation method compared to the manual segmentation for cases A and B. The mean Dice Similarity Coefficient for the ITK-SNAP and the GC-prior methods are 0.91 and 0.9, respectively.

timepoint. As shown in Fig. 3(c), the validation study results show that the predicted shape prior may deviate from the actual computed iceball at any timepoint. This expected deviation is caused by the error introduced in the probes' identification, the error made in the first-order assumption of simple iceball summation from multiple probes, and error from the influence of perfusion from local blood vessels on the iceball's shape. Nonetheless, we see from Fig. 3(g) and Fig. 4 that our accurate segmentation results are still strongly dependent on the intensity information, with the shape prior providing the bias among different cases, which is a sign of our method's robustness.

V. CONCLUSIONS

We developed a fully automatic segmentation method to extract the cryoablation iceball from time series of 3D images during the first freeze cycle in kidney ablations. Our method incorporates shape prior information into the standard graph cuts segmentation framework in order to separate the iceball from nearby anatomy with similar intensity values. The shape prior is generated by modeling the growth of the iceball using experimentally derived parameters. No training data set is necessary. We compared the segmentation results of our approach and other semi-automatic segmentation methods for 8 timepoints in 2 cases, and the results suggest that our method is accurate and robust.

REFERENCES

[1] P.A. Yushkevich, J. Piven, H.C. Hazlett, R.G. Smith, S. Ho, J.C. Gee and G. Gerig, User-guided 3D active contour segmentation of anatomical structures: significantly improved efficiency and reliability, Neuroimage, 31(3):1116-28, 2006.

[2] E. Pichon, A. Tannenbaum and R. Kikinis. A statistically based flow for image segmentation, Med. Image Anal., 8(3):267-74, 2004.

[3] D. Greig, B. Porteous and A. Seheult, Exact maximum a posteriori estimation for binary images, Journal of the Royal Statistical Society, Series B, 51(2):487–496, 1989.

[4] Y. Boykov and V. Kolmogorov, An experimental comparison of min-cut/max-flow algorithms for energy minimization in vision, IEEE Transactions on Pattern Analysis and Machine Intelligence, vol. 26(9), pp. 1124–1137, 2004.

[5] Y. Boykov and G. Funka-lea, Graph cuts and efficient n-d image segmentation, International Journal of Computer Vision, 70(2):109–131, 2006.

[6] J. Malcolm, Y. Rathi and A. Tannenbaum, Graph cut segmentation with nonlinear shape priors, International Conference on Image Processing (ICIP), 2007

[7] D. Freedman and T. Zhang, Interactive graph cut based segmentation with shape priors, Computer Vision and Pattern Recognition (CVPR), 2005